PGL germ granule assembly protein is a base-specific, single-stranded RNase

Scott T. Aoki[a], Aaron M. Kershner[b,1], Craig A. Bingman[a], Marvin Wickens[a], and Judith Kimble[a,b,2]

[a]Department of Biochemistry, University of Wisconsin–Madison, Madison, WI 53706; and [b]Howard Hughes Medical Institute, University of Wisconsin–Madison, Madison, WI 53706

Contributed by Judith Kimble, December 21, 2015 (sent for review December 5, 2015; reviewed by Anne Ephrussi, Harry F. Noller, and Susan Strome)

Cellular RNA-protein (RNP) granules are ubiquitous and have fundamental roles in biology and RNA metabolism, but the molecular basis of their structure, assembly, and function is poorly understood. Using nematode "P-granules" as a paradigm, we focus on the PGL granule scaffold protein to gain molecular insights into RNP granule structure and assembly. We first identify a PGL dimerization domain (DD) and determine its crystal structure. PGL-1 DD has a novel 13 α-helix fold that creates a positively charged channel as a homodimer. We investigate its capacity to bind RNA and discover unexpectedly that PGL-1 DD is a guanosine-specific, single-stranded endonuclease. Discovery of the PGL homodimer, together with previous results, suggests a model in which the PGL DD dimer forms a fundamental building block for P-granule assembly. Discovery of the PGL RNase activity expands the role of RNP granule assembly proteins to include enzymatic activity in addition to their job as structural scaffolds.

germ-cell development | PGL-1 | PGL-3 | P-granules | RNA endonuclease

Cytoplasmic RNA-protein (RNP) granules are found in virtually all cells and are thought to be central to RNA metabolism (1, 2). These diverse organelles include P-bodies, stress granules, neuronal granules, and germ granules (2). RNP granules are not membrane-bound and display liquid–liquid phase-separation properties (3, 4). Many of their molecular components have been identified, including scaffold proteins: proteins that recruit other key granule components and are sufficient to induce RNP granule assembly. Major challenges now are to understand how RNP granules are assembled and how they control RNAs.

Germ granules are exemplary RNP granules with a profound yet largely mysterious role in metazoan germ-line development. These granules possess common components across phyla (5) but use unique scaffold proteins, such as *Drosophila* Oskar (6), zebrafish Bucky Ball (7), and *Caenorhabditis elegans* paralogs PGL-1 and PGL-3 (8, 9), called PGL collectively. Germ granule scaffold proteins from different phyla have distinct amino acid sequences with no conserved domains. The importance of these scaffolds has been attributed to their function in germ granule assembly (for examples, see refs. 10–12). However, the molecular basis of that assembly and how it impacts RNA regulation remain unknown.

Here we focus on the *Caenorhabditid* PGL scaffold proteins and their role in assembly of nematode germ granules, called P-granules (13). P-granules are required for germ-line survival (8, 9) and germ-line totipotency (14). A recent model proposes that P-granules capture selected mRNAs exiting the nucleus (15), an idea based on the finding that untranslated mRNAs are enriched in P-granules, but translated mRNAs are absent (15, 16). The consequences of that capture are unclear but may include mRNA repression.

The PGL family comprises the closely related PGL-1 and PGL-3 proteins plus divergent PGL-2. PGL-1 and PGL-3 are required for adult germ cell development but the function of PGL-2 is unknown (8). All three PGL proteins interact with each other in vitro (8), but thus far only PGL-1 and PGL-3 are known to self-assemble into granules when expressed in nematode somatic cells or in mammalian cell culture (17, 18). By primary sequence prediction, PGLs have only one recognizable region, C-terminal RGG repeats (Fig. 1*A*) (8, 9), which are associated with protein turnover and RNA binding (17, 19). In non-PGL proteins, RGG repeats can recruit RNA binding proteins (20) and facilitate in vitro granule formation (21). Experiments in tissue culture cells implicate the N-terminal half of the PGL protein—but not the RGG repeats—in P-granule assembly (17). Whereas full-length PGL-3 self-assembled, a mutant lacking ∼160 residues from the PGL-3 N-terminal half (Fig. 1*A*) no longer formed granules (17). Thus, in-roads have been made but molecular detail about how PGL organizes itself into a granule is lacking.

Here we identify a PGL dimerization domain (DD) and propose that PGL dimers are a key building block for P-granule assembly. We determine the PGL-1 DD crystal structure and find a novel 13-helix fold that creates a positively charged channel as a homodimer. Testing the idea that this channel might bind RNA, we discovered that PGL DD is an RNase and determined PGL-1 DD's specificity in vitro for guanosine in single-stranded RNAs. We suggest that PGL DD has a dual role in P-granules, as a domain essential for assembly and as an RNase.

Results

PGL Dimerization and Its Crystal Structure. We biochemically characterized the PGL proteins to better understand regions contributing to granule assembly. Amino acid sequence alignments identified a large region spanning the N-terminal two-thirds of the protein that was conserved among *Caenorhabditids* (Fig. 1*A* and *Materials and*

Significance

RNA-protein granules play crucial roles in cell biology, development, and disease. Yet their molecular assembly and biochemical functions remain poorly understood. This work focuses on a granule scaffold protein, called PGL, to gain molecular insights into granule assembly and function. We identify a dimerization domain in a PGL region required for granule assembly and determine its crystal structure. The structure reveals a positively charged channel of the right size for binding single-stranded RNA. However, we instead find that PGL is a base-specific RNA endonuclease. The importance of this work lies in its molecular clarification of a building block for granule assembly and discovery of an activity that provides a new view of a scaffold protein as an enzyme.

Author contributions: S.T.A., A.M.K., and M.W. designed research; S.T.A., A.M.K., and C.A.B. performed research; S.T.A., A.M.K., C.A.B., M.W., and J.K. analyzed data; and S.T.A., M.W., and J.K. wrote the paper.

Reviewers: A.E., European Molecular Biology Laboratory; H.F.N., University of California, Santa Cruz; and S.S., University of California, Santa Cruz.

The authors declare no conflict of interest.

Data deposition: The atomic coordinates and structure factors have been deposited in the Protein Data Bank, www.pdb.org [PDB ID code 5COW for *Caenorhabditis remanei* PGL-1 DD, native; PDB ID code 5CV3 for *C. remanei* PGL-1 DD, Thimerosal (Hg); and PDB ID code 5CV1 for *Caenorhabditis elegans* PGL-1 DD].

[1]Present address: Department of Biochemistry and Institute of Stem Cell Biology and Regenerative Medicine, Stanford University, Stanford, CA 94305.

[2]To whom correspondence should be addressed. Email: jekimble@wisc.edu.

This article contains supporting information online at www.pnas.org/lookup/suppl/doi:10.1073/pnas.1524400113/-/DCSupplemental.

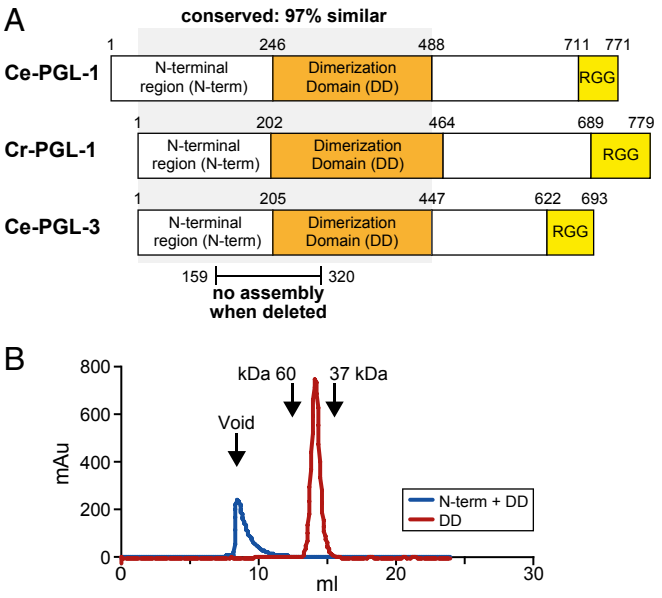

Fig. 1. Identification of the PGL dimerization domain. (*A*) *C. elegans* PGL-1, PGL-3, and *C. remanei* PGL-1 protein schematic. The only recognizable motif by sequence prediction is the RGG repeat region (yellow). The region implicated in granule formation (17) is shown here below PGL-3. We first identified the DD (orange) in PGL-3 (see main text). (*B*) Size-exclusion chromatography of *C. elegans* PGL-3 recombinant protein "N-term + DD" (blue) and "DD" (red). Arrows indicate positions of the void volume, albumin (60 kDa), and MBP (37 kDa).

Methods). Our initial characterization focused on purified recombinant *C. elegans* PGL-3 (*Ce*-PGL-3) (Fig. S1*A*). *Ce*-PGL-3 residues 1–447 ran in the void on a sizing column (Fig. 1*B*) and multimerized in chemical cross-linking experiments (Fig. S1*B*), consistent with that fragment assembling into a large multimer. Limited proteolysis of *Ce*-PGL-3 residues 1–447 identified a single protected fragment (Fig. S1*C*). N-terminal sequencing and additional proteolysis mapped the fragment to residues 205–447 (Fig. 1*A*). This 25-kDa domain dimerized in solution, as determined by both size-exclusion chromatography (Fig. 1*B*) and chemical cross-linking (Fig. S1*D*). We therefore refer to this region as the PGL DD.

To gain molecular insight into PGL DD dimerization, we determined crystal structures of *C. elegans* (*Ce*) and *Caenorhabditis remanei* (*Cr*) PGL-1 DD to 3.6 Å and 1.6 Å, respectively (Table S1; more details in *Materials and Methods*). Both structures revealed a domain of 13 α-helices that assume an identical, novel fold (Fig. 2*A* and Fig. S2 *A* and *B*) (RMSD = 0.826 Å). A similar structure could not be found with protein fold-alignment software (Dali) (22), consistent with primary sequence alignments reporting PGLs as novel proteins. *Cr*- and *Ce*-PGL-1 DD both crystallized as single subunits in their asymmetric unit (Fig. 2*A* and Fig. S2 *A* and *B*). Therefore, the asymmetric unit on its own could not be used to identify the biologically relevant dimer. We instead analyzed the crystal packing of both structures to see whether the dimer crystallized on a crystal symmetry axis. Our two crystal structures are of different PGL-1 homologs and have completely different space groups, but have only one conserved protein–protein interface between them (Fig. 2*B* and Fig. S2*C*). A similar dimerization-fold was calculated by PISA (23), an assembly-prediction program. Thus, both proteins crystallized as identical homodimers on different twofold crystal symmetry axes, providing convincing evidence that this is the authentic dimer structure.

The PGL-1 DD dimer makes extensive subunit contacts. For example, the higher resolution *Cr*-PGL-1 DD dimer interface has a large buried surface area (1,239 Å^2) that is predicted to form a combined total of 13 hydrogen bonds and salt bridges (PISA) (Fig. 2*C*). Importantly, the dimer-interface residues are highly conserved between PGL-1 and PGL-3 homologs (Fig. 2*D*). However, those residues are not as well conserved in PGL-2 (Fig. S2*D*).

PGL-1 DD dimerization forms a central channel between its subunits (Fig. 2*B* and Fig. S2*C*). The N-terminal half of PGL-1 DD makes most of the dimer interactions (10 of 13 total hydrogen bonds and salt bridges, *Cr*-PGL-1 DD) to form the top of the channel. In contrast, helix α11 in the C terminus makes minimal contacts with its counterpart in the adjacent subunit (3 of 13 total hydrogen bonds and salt bridges, *Cr*-PGL-1 DD) to enclose the channel at the bottom (Fig. 2*B* and Fig. S2*C*). The asymmetry between the number of contacts at the top and bottom of the channel implies that the relatively weak α11:α11 interaction may be dynamic and permit access to the channel interior without disrupting dimerization. The channel diameter, measured from C-α traces of its surrounding helices, is roughly 15 Å, providing sufficient room for single-stranded—but not double-stranded—nucleic acid. Moreover, the electrostatic surface potential of the channel is basic (Fig. 2*E*). We postulate that the PGL-1 DD dimer may accommodate RNA within its channel, given the channel size, surface charge, and the established relationship between P-granules and RNA. Thus, the PGL-1 DD structure provides insight into its dimerization and also suggests a possible second role, previously not considered, as an RNA binding domain.

PGL-1 Is a Guanosine-Specific Endonuclease. To test the idea that PGL DD binds RNA, we used EMSA, in which stable RNA–protein complexes migrate more slowly than free RNA. However, the opposite was observed. When *Ce*-PGL-1 DD was incubated with 5′ labeled RNAs, the RNA migrated faster than RNA alone (Fig. 3*A*).

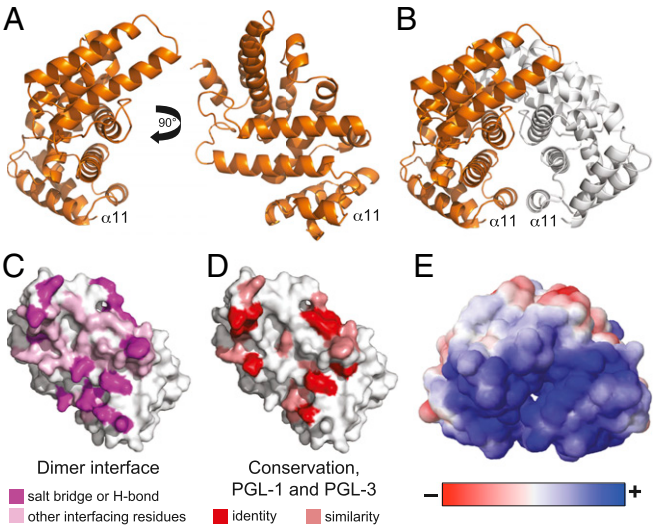

Fig. 2. Crystal structure of the *C. remanei* PGL-1 dimerization domain. (*A*) *C. remanei* PGL-1 (*Cr*-PGL-1) DD crystal structure to 1.6 Å (PDB ID code 5COW). Structure represents *Cr*-PGL-1 amino acids 202–464 with amino acids 321–335 removed. See Table S1 for data statistics and Fig. S2*A* for *C. elegans* PGL-1 DD crystal structure. Helix labeled "α11" encloses the dimer channel in *B*–*E*. (*B*) *Cr*-PGL-1 DD dimer. See main text for explanation. Subunits in orange and gray. (*C*) *C. remanei* PGL-1 DD dimer interface. Salt bridge and hydrogen (H-) bond residues in magenta; other interacting residues that are closely apposed, including hydrophobic residues, in pink. (*D*) Conservation of dimer interfacing residues by identity (red) and similarity (salmon), as assessed by sequence alignments with PGL-1 homologs, including PGL-3. This analysis does not include interface residues capable of coordinating water molecules between the two subunits. (*E*) Electrostatic potential of *Cr*-PGL-1 DD dimer. Color intensity correlates with degree of estimated positive (blue, +) or negative (red, –) charge. Image generated by PDB2PQR (39).

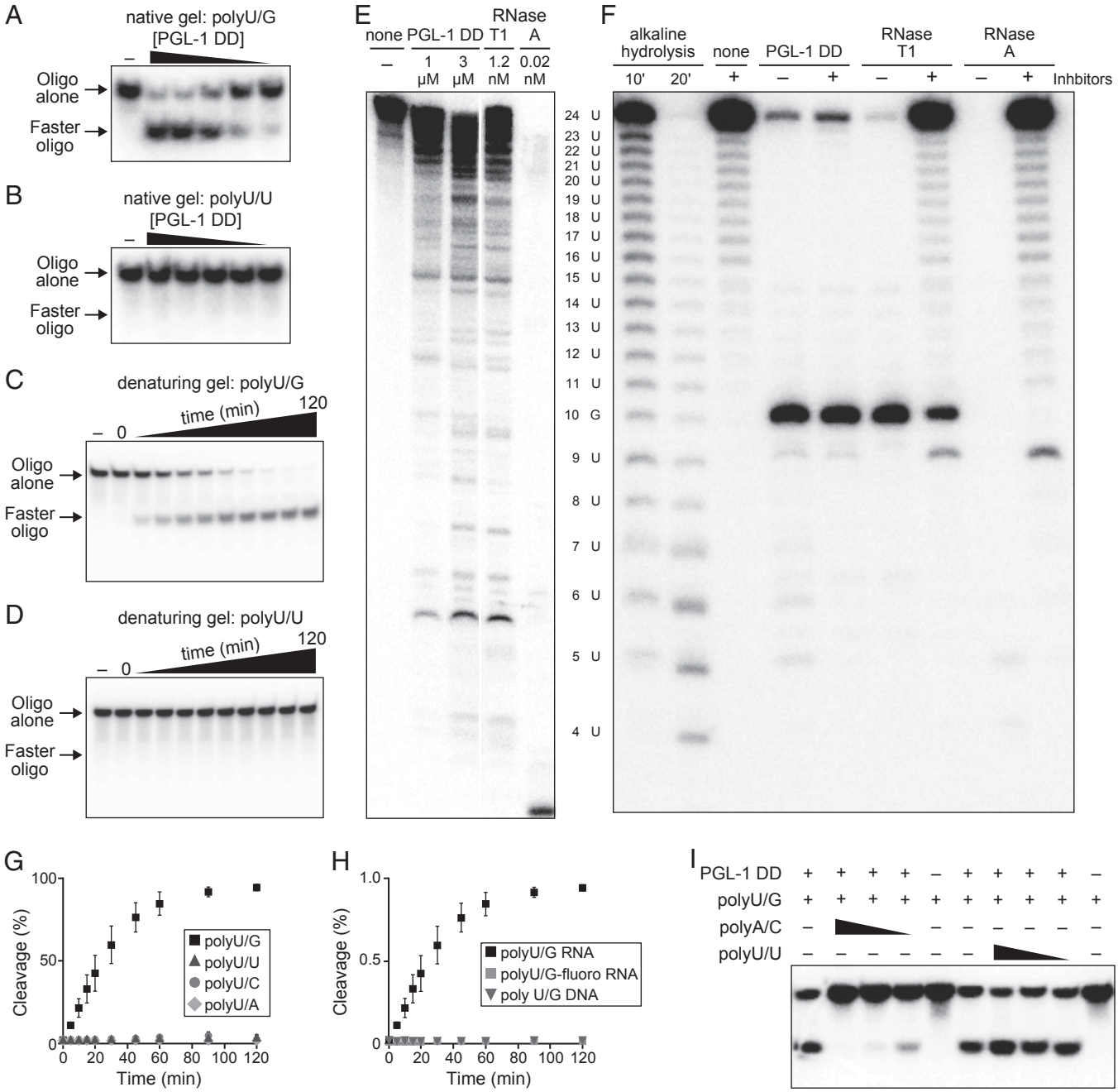

Fig. 3. PGL DD is a guanosine-specific, single-stranded RNA endonuclease. In *A–D* and *F–I*, recombinant MBP::*Ce*-PGL-1 DD (PGL-1 DD) was incubated with 5′ ^{32}P-labeled RNA oligos and assayed for RNA cleavage products at room temperature (~20 °C). Substrates were polyX/Y, where X refers to the major base of the oligo and Y refers to a single base at an interior site (Table S2). All nucleic acid oligos were 24 bases long, with the interior site at base number 10. (*A* and *B*) Native gels of different RNA oligos (*1 nM) incubated for 1 h with decreasing concentrations of PGL-1 DD (3–0.03 μM). "–" indicates when RNA was incubated for 1 h without PGL-1 DD. The "faster oligo" is observed with (*A*) polyU/G but not with (*B*) polyU/U RNA. (*C* and *D*) Denaturing gels run after time-course incubation of RNA with 1 μM PGL-1 DD. "0" indicates when sample was immediately taken after addition of PGL-1 DD. "–" indicates when RNA was incubated for 120 min without PGL-1 DD. (*C*) With polyU/G RNA as a substrate, increasing amounts of cleavage product ("faster oligo") appear with increasing times of DD incubation. (*D*) With polyU/U RNA as a substrate, no cleavage product is observed upon DD incubation. (*E* and *F*) Comparison of PGL-1 DD enzymatic activity with characterized RNases. (*E*) RNA cleavage with PGL-1 DD and commercial RNases. Denaturing gel of in vitro-transcribed ^{32}P-guanosine-labeled *pos-1* 3′UTR (315 bases) (Table S2) incubated with PGL-1 DD (1 and 3 μM), RNase T1 (1.2 nM), or RNase A (0.02 nM) for 1 h; "none" indicates sample incubated without recombinant protein or RNase. PGL-1 DD (3 μM) produces a similar cleavage pattern to RNase T1 (1.2 nM), an ~2,500-fold concentration difference. RNase A (0.02 nM) completely degrades the radiolabeled RNA. (*F*) Higher-resolution gel of RNase cleavage products and enzyme sensitivity to inhibitors. Denaturing gel of polyU/G RNA (*10 nM) incubated with PGL-1 DD (1 μM), RNase T1 (1.2 nM), and RNase A (0.02 nM) for 1 h; "none" indicates sample incubated without RNase. Sample incubated without ("–") or with ("+") RNase inhibitors. Alkaline hydrolysis fragmentation of polyU/G RNA used to generate a ladder for cleavage product size approximation. (*G*) One micromolar PGL-1 DD incubated with polyuridine RNA oligos (*1 nM) containing four different interior RNA bases (guanosine, uridine, cytidine, and adenosine) and sampled over time. (*H*) One micromolar PGL-1 DD incubated with polyU/G RNA, polyU/G RNA with 2′-fluorinated guanosine ("polyU/G-fluoro") and polyU/G DNA ("DNA"), all at *1 nM. Cleavage percentage in (*G* and *H*) calculated as (cleavage product)/[(uncleaved oligo) + (cleavage product)] from measured band density. Average values and SDs of RNase cleavage determined from three separate experiments. (*I*) Cleavage gel of polyU/G RNA (*1 nM) incubated with complementary polyA/C or polyU/U RNAs in 10:1,1:1, 0.1:1 estimated molar ratios (ramp) before the addition ("+") of PGL-1 DD. "–" indicates when protein or RNA were excluded from the reaction. *Oligo concentration prior to 5′ radiolabeling.

The faster RNA migration on native gels implied a decrease in RNA size, which was validated on denaturing gels (Fig. 3*C*). Thus, PGL-1 DD cleaves RNA. RNA cleavage was also found for *Ce*-PGL-3 and *Cr*-PGL-1 (Fig. S3 *A* and *B*), demonstrating conservation of this enzymatic activity among closely related PGL proteins.

Ce-PGL-1 DD cleaved certain RNAs but not others (Fig. 3 *A*–*D*), implying specificity for sequence, or secondary or tertiary structure. Incubation of *Ce*-PGL-1 DD with a longer and more complex RNA (*pos-1* 3′UTR, 315 bases) yielded a cleavage pattern similar to that of RNase T1 (Fig. 3*E*), a guanosine-specific RNA endonuclease that cleaves 3′ to guanosines (24). PGL-1 DD incubation with a polyuridine RNA oligo harboring a single interior guanosine base (polyU/G) enriched for a single cleavage product identical in size to that produced by RNase T1 (Fig. 3*F*). In contrast, incubation with RNase A, a pyrimidine-specific RNase (25), caused complete degradation (Fig. 3*F*). Inclusion of commercial RNase inhibitors suppressed enzymatic activity of RNase T1 and A, but had no observable effect on PGL DD cleavage (Fig. 3*F*), arguing against an RNase contaminant being responsible for the PGL DD cleavage result. These findings, along with our crystal structures showing a novel fold, suggest that PGL DD is a new endonuclease.

The size similarity between the cleavage products of PGL-1 DD and T1 endonucleases led us to explore further the PGL-1 DD RNase specificity. We tested the ability of PGL-1 DD to cleave a polyuridine RNA harboring other single-base changes within the oligo. No RNA cleavage was observed upon inclusion of uridine, cytidine, and adenosine bases (Fig. 3*G*), whereas cleavage occurred in a concentration-dependent manner with guanosine (Fig. 3*G* and Fig. S3*C*). Because the uridine base pairs with adenosine, we also tested a polyadenine RNA oligo with an interior cytosine base (polyA/C) but similarly observed no cleavage (Fig. S3*D*). We next explored ways to inhibit PGL-1 DD cleavage of its guanine-containing substrate. RNA endonucleases cleave RNA using its 2′ hydroxyl, not found in DNA, for nucleophilic attack (26). PGL-1 DD could not cleave a DNA polyU/G oligo, nor an RNA polyU/G oligo with a 2′ hydroxyl modified to 2′ fluorinated guanosine (Fig. 3*H*). Therefore, PGL-1 DD specifically cleaves guanosine-containing RNA. PGL DD may have additional, unexplored RNA target-sequence specificity other than guanosine, and may be like RNase T1, whose catalytic rates are greatly affected by the base adjacent to guanosines (27). PGL binding partners, particularly those that bind RNA, such as IFE-1 (12), may modify the PGL DD RNase activity. We next tested for secondary-structure specificity. The diameter of the PGL DD dimer channel is predicted to fit only single-stranded RNA (see above), assuming no significant structural rearrangement. In support of a restriction to single-stranded RNA, cleavage was also blocked by preincubation of polyU/G with its complementary oligo (polyA/C) to form double-stranded RNA (Fig. 3*I*). Addition of a noncomplementary polyuridine RNA oligo had no effect on cleavage (Fig. 3*I*). Taken together, our results suggest that PGL-1 DD is a guanosine-specific, single-stranded RNA endonuclease.

What residues mediate the PGL DD enzymatic activity? Ribonucleases have a diversity of domains that form active sites with a similar molecular composition (26). Cleavage is typically accomplished through acid/base chemistry via amino acid side chains or divalent metals (26). Cleavage by PGL-1 DD is not likely to rely on a common divalent metal, because all cleavage assays were done in the presence of a metal chelator (EDTA) and addition of common metals (Mg, Mn) did not significantly affect cleavage rates (Fig. S4*A*). Other metals (e.g., Co, Cu) caused protein precipitation and could not be adequately tested. In metal-independent RNases, like RNase T1, histidine typically serves as the base in the active site, and is paired with either another histidine or an acidic side chain (26). We found only a single conserved histidine paired with a neighboring acidic side chain, a glutamate (Fig. S4 *B*–*D*). Mutation of this histidine reduced RNA cleavage activity significantly (Fig. S4*E*), but mutation of its pairing glutamate had no effect (Fig. S4*E*). Therefore, PGL DD is unlikely to have a classic RNase active site.

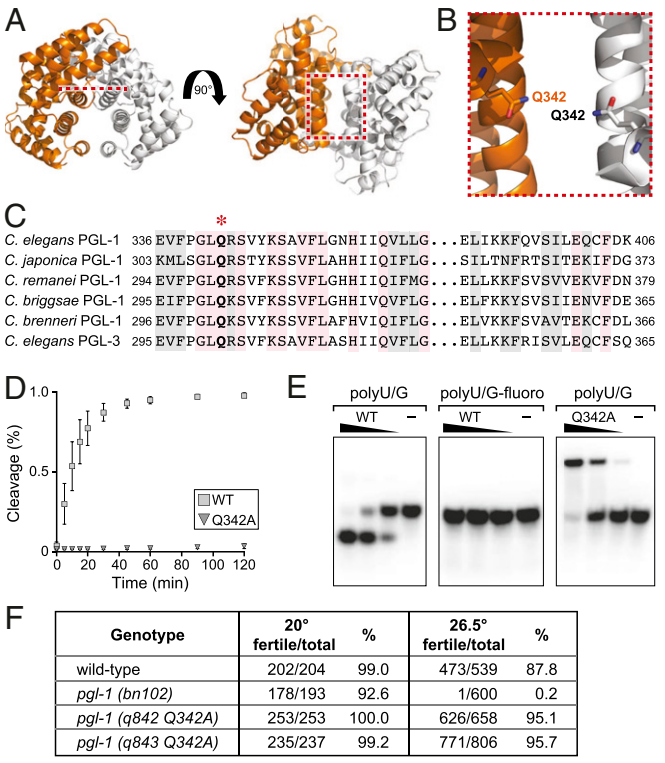

F

Genotype	20° fertile/total	%	26.5° fertile/total	%
wild-type	202/204	99.0	473/539	87.8
pgl-1 (bn102)	178/193	92.6	1/600	0.2
pgl-1 (q842 Q342A)	253/253	100.0	626/658	95.1
pgl-1 (q843 Q342A)	235/237	99.2	771/806	95.7

Fig. 4. A glutamine mutation abrogates PGL-1 endonuclease activity. (*A*) Location of the relevant glutamine in the *Cr*-PGL-1 DD dimer. When oriented along the channel, the PGL-1 DD dimer subunits assemble antiparallel to each other. Red line shows the plane of the red box in adjacent orthogonal view. Red box identifies structural region enlarged in *B*. (*B*) Atomic detail of Q342 in the *Cr*-PGL-1 DD dimer. Numbering corresponds to *Ce*-PGL-1. (*C*) Sequence conservation of Q342 ("*") among *Caenorhabditid*. (*D*) PGL-1 Q342A abrogates cleavage activity. Cleavage efficiency assessed with 3 μM MBP::*Ce*-PGL-1 DD wild-type and Q342A mutant protein, and a polyU/G RNA oligo (Table S2). Cleavage percentage calculated as in Fig. 3 *G* and *H*. (*E*) PGL-1 Q342A still binds RNA. Native gels of 5′ ^{32}P-labeled RNA incubated for 30 min without ("–") or with 3–0.3 μM (ramp) MBP::*Ce*-PGL-1 DD wild-type (WT) or RNase mutant (Q342A). In all panels, recombinant protein was incubated with *1 nM 5′ ^{32}P-labeled polyU/G or 2′ fluorinated polyU/G ("polyU/G-fluoro") (see main text and Table S2) RNA oligos before running on a native gel. "–" identifies RNA incubated without PGL-1 DD. *Oligo concentration prior to 5′ radiolabeling. (*F*) Lack of biological effect in *pgl-1* Q342A mutants. Wild-type, *pgl-1*–null and two independent *pgl-1* Q342A RNase mutants were singled and scored for fertility after incubation at either 20 °C or 26.5 °C, as performed in ref. 8. More details in *SI Materials and Methods*.

We sought other residues that might mediate catalysis. At the top of the channel, within a solvent-exposed region of the dimer subunit interface (Fig. 4 *A* and *B*), a conserved glutamine in one subunit comes together with its counterpart in the other subunit (Fig. 4 *A*–*C*). Mutation of that glutamine to alanine (*Ce*-PGL-1 Q342A) abolished PGL-1 DD cleavage activity (Fig. 4*D*) but did not affect dimerization (Fig. S5). Moreover, unlike the wild-type protein, incubation of the PGL-1 Q342A mutant protein with polyU/G slowed migration of the labeled oligo (Fig. 4*E*). This slower migrating band likely represents a PGL-1 DD–RNA complex and indicates that PGL-1 Q342A binds RNA. We conclude that PGL-1 Q342A abrogates RNase activity without affecting dimerization or RNA binding. The glutamine could be part of the active site, coordinate an untested metal, or affect function allosterically through local misfolding. Access to Q342 requires either dimer subunit separation or entry into the channel. We speculate therefore that the dimer channel is crucial for RNA interaction and enzyme catalysis. Regardless, the PGL-1 Q342A mutant demonstrates that PGL-1 DD is responsible for the observed RNase activity, and excludes

the notion that this activity is a contaminant from recombinant protein purification or the environment.

To test the role of PGL-1 RNase activity in vivo, we used CRISPR/Cas9 gene editing to generate two independent but identical Q342A RNase defective mutations in the endogenous *C. elegans pgl-1* locus (*Materials and Methods*). Wild-type worms were fertile at 20 °C and 26.5 °C; in contrast *pgl-1*–null mutants were fertile only at 20 °C but sterile at 26.5 °C (Fig. 4*F*) (9). Unlike the *pgl-1*–null mutant, both *pgl-1* Q342A mutants were fertile at both 20 °C and 26.5 °C (Fig. 4*F*). Therefore, PGL-1 RNase activity is likely not required for its role in fertility.

Discussion

This work reveals two key features of PGL proteins: the PGL dimerization domain and PGL-1 guanosine-specific RNA endonuclease activity. Discovery of the PGL dimerization domain allows us to expand on the Hanazawa model for P-granule assembly (17) to include PGL DD as a fundamental building block of the P-granule scaffold. Hanazawa et al. found a PGL deletion that eliminates granule assembly (Fig. 1*A*) (17), and we now know that their deletion removes part of PGL DD. Putting PGL dimerization (present work) together with PGL multimerization (17), we now suggest that the P-granule framework is constructed from multimers of PGL dimers. This strategy is similar in nature to that of Oskar, the fly germ granule scaffold protein that also dimerizes to facilitate assembly (28).

Discovery of the PGL RNase activity changes our view of RNP granule scaffold proteins. Previously, only the RGG repeats linked the PGL scaffold with RNA (17). The PGL DD RNA endonuclease activity was unexpected. Its structure assumes a novel fold and lacks any cluster of amino acids recognizable as a classic RNase active site, which opens a host of questions about its enzyme mechanism, base specificity, P-granule function, regulation, and conservation. PGL's enzymatic activity is modest compared with classic guanosine-specific RNases, like RNase T1. PGL could have additional sequence specificity not yet identified, or specificity for a modified guanosine, like the 5′ cap. Alternatively, inefficiency may be ideal for a granule-forming enzyme to permit RNase activity only when present at high concentrations within P-granules.

Enzymatic activities in other germ granule scaffold proteins, zebrafish Bucky Ball and *Drosophila* Oskar, have not been identified, but it is plausible that they, like PGL, may contain novel enzymatic domains or recruit enzymes to serve analogous roles. Intriguingly, Maelstrom, a Piwi-interacting RNA (piRNA) biogenesis factor and germ-granule component, was recently identified as a novel guanosine RNase (29). The RNA targets of the Maelstrom nuclease are unknown and its enzymatic activity is dispensable in vivo for piRNA biogenesis. Although Maelstrom and PGL are structurally unrelated, their parallels are striking: both reside in germ granules, both possess guanosine RNA endonuclease activity, and that enzymatic activity is dispensable in vivo. An attractive idea is that convergent evolution established RNase activity in distinct proteins within germ granules and that their activities serve a common purpose in reproduction.

What might the PGL RNase do in P-granules? Selected mRNAs localize to P-granules and that localization correlates with their translational inhibition (16). PGL DD RNase may cleave the 5′ cap or 3′ regulatory regions of mRNAs retained in P-granules, and hence block translation. Potential targets include genes associated with neuronal and muscle cell development, which are inhibited in P-granules to prevent aberrant germ cell differentiation (14). The RNases responsible for piRNA biogenesis are largely unknown and those that are known have no obvious homologs (30). For example, Zucchini, a piRNA biogenesis RNase, has no known nematode equivalent. PGL may be the functional counterpart of Zucchini or play some other role in piRNA metabolism. Regardless, the insights from this work provide a starting point to further explore the molecular assembly and RNA regulatory mechanisms of this model RNP granule.

Materials and Methods

Additional details can be found in the *SI Materials and Methods*.

Protein Construct Design. Sequence alignments were generated by T-Coffee (31) to identify a conserved N-terminal region (*C. elegans* PGL-1 amino acid residues 42–488). *C. elegans* PGL-1 and PGL-3 constructs were generated by PCR amplification of *C. elegans* N2 cDNA. The *C. remanei* DD protein-expression construct was codon-optimized for *Escherichia coli* expression and assembled with gBlocks (IDT Technologies) by Gibson cloning (32). For maltose binding protein (MBP)-tagged *C. elegans* DD domain protein constructs, MBP was PCR-amplified from a pMAL-c2x plasmid (New England Biolabs).

Protein Purification. Details regarding protein purification can be found in *SI Materials and Methods*. Purification was finished on a S200 size-exclusion column (GE Healthcare) in PGL buffer [20 mM Hepes pH 7.0, 50 mM NaCl, 0.5 mM Tris(2-carboxyethyl)phosphine pH 7.0 (TCEP, Sigma)]. FPLC fractions were again analyzed by SDS/PAGE and Coomassie staining. Peak fractions were concentrated with a 10K cut-off Amicon Ultra-4 concentrator (EMD Millipore) and stored at 4 °C until use. Final protein concentration was estimated by A280. See Fig. S5*B* for an example of the final protein used in RNA experiments.

Protein Cross-Linking and Protease Digestion Analyses.

Cross-linking. Bis[sulfosuccinimidyl] suberate (BS3, Pierce) was diluted in cross-linking buffer (20 mM Hepes pH 7.0, 150 mM NaCl) and added to recombinant protein for a final concentration of 10 μM protein and 2-, 7-, 22-, 67-, 200-μM cross-linker. Buffer alone was added as a negative control. The reaction was quenched with Tris pH 8.0 (50-mM final concentration). Samples were analyzed by SDS/PAGE and Coomassie staining.

Protease digestion. Proteomics-grade Trypsin (1 μg/mL final concentration; Sigma-Aldrich) was added to recombinant PGL-3 residues 1–447 (0.4 mg/mL) and samples were taken at 5, 10, 20, 40, and 60 min, and before the addition of trypsin as a negative control. Samples were analyzed by SDS/PAGE and Coomassie staining. SDS/PAGE gels were also transferred to PVDF, and submitted for N-terminal sequencing (Tufts University Core Facility, M. Berne).

Protein crystallization and structure determination. Final crystal conditions for *C. elegans* PGL-1 DD were 1.575–1.625 M sodium malonate pH 5.9, 50–100 mM GuCl, 1 mM TCEP, 1 mM sodium azide. The dataset submitted was from a crystal soaked in gadolinium chloride (10 mM) overnight before freezing. Diffraction data were collected at the Life Sciences-Collaborative Access Team (LS-CAT) and The National Institute of General Medical Sciences and National Cancer Institute Structural Biology Facility (GM/CA). A complete dataset could only be collected to 3.6 Å in space group $P6_1$ 2 2. The *C. remanei* PGL-1 DD Δloop crystals that diffracted best were in [100 mM Pipes pH 6.0, 24–27% (wt/vol) PEG 4000, 200 mM LiSO4, 1 mM TCEP, 1 mM sodium azide]. We could obtain single-wavelength anomalous dispersion phase information from a Thimerosal soaked crystal (10 mM, 24 h) to 3.6 Å. Diffraction data for *C. remanei* crystals were collected at LS-CAT and Advanced Light Source (ALS)/Howard Hughes Medical Institute (HHMI). Data processing was performed in HKL2000 (33), model building done in Coot (34), and refinement in *PHENIX* (35). The final *C. remanei* model was used for model phases in the *C. elegans* dataset. Molecular replacement was performed by *Phaser* (36). Final structure statistics are found in Table S1. Datasets, structure models, and additional information can be found in the RCSB Protein Data Bank. The PDB IDs are as follows: *C. remanei* PGL-1 DD, native (PDB ID code 5COW); *C. remanei* PGL-1 DD, Thimerosal (Hg) (PDB ID code 5CV3); *C. elegans* PGL-1 DD (PDB ID code 5CV1).

Nucleic acid labeling. RNA and DNA oligos were commercially synthesized (Table S2) (IDT Technologies). The 5′ labeling with ^{32}P was done with phosphonucleotide kinase (New England Biolabs) and EasyTide ^{32}P γ-ATP (Perkin-Elmer). A plasmid of *pos-1* mRNA with 3′UTR was cloned from mixed stage N2 and transcribed using the AmpliScribe T7-Flash Transcription Kit (Epicentre) with GTP in rate-limiting quantities to promote incorporation of ^{32}P α-GTP (Perkin-Elmer). The RNA transcript was gel-purified.

Native gel shifts. polyU/G RNA was incubated with MBP::PGL-1 DD at designated concentrations in cleavage buffer (10 mM Hepes pH 7.0, 50 mM NaCl, 1 mM EDTA, 1 mM DTT, 0.1 mg/mL BSA, 0.1% Tween-20) for 30 min at room temperature. In the case of metal cleavage assays, 1 μM MBP::PGL-1 DD was incubated with 5 mM EDTA, 5 mM $MgCl_2$, or 5 mM $MnCl_2$ for 30 min at room temperature. The 6X EMSA Gel Loading Buffer [15% (wt/vol) Ficoll (400,000 Da), 0.01% Bromophenol blue] was added to samples and run on a 5% TBE native gel (Bio-Rad). Gels were dried exposed to a phosphoscreen (Kodak) for 24 h. Phosphoscreens were developed on a Typhoon 9000 (GE Healthcare) and images were obtained using ImageQuant (GE Healthcare).

pos-1 and RNA oligo digestion. Purified ^{32}P-labeled *pos-1 3′* UTR RNA was incubated with *C. elegans* MBP::PGL-1 DD (1 and 3 μM), RNase T1 (1.2 nM; Thermo

Scientific), RNase A (0.02 nM; Sigma-Aldrich), and a negative control (dH_20) in cleavage buffer for 1 h at room temperature (~20 °C). Samples were phenol-chloroform extracted, and run on a 0.75-mm 15% (vol/vol) urea-TBE gel (National Diagnostics). Gels were fixed, dried, and developed similar to the native gels. ^{32}P-labeled PolyU/G RNA oligonucleotide (Table S2) was incubated with *C. elegans* MBP::PGL-1 DD (1 μM), RNase T1 (1.2 nM), RNase A (0.02 nM), and a negative control (dH_20) in cleavage buffer for 1 h at room temperature. Samples were phenol-chloroform–extracted and run on a 20% (vol/vol) urea-TBE gel and analyzed similar to that described in *pos-1* RNA digestion analysis. Both experiments were repeated at least three times with similar results.

Time-course digestion assays. ^{32}P-labeled RNA and DNA oligonucleotides (1 nM, based on oligo concentration before ^{32}P-labeling) were incubated with varying concentrations of *C. elegans* MBP::PGL-1 DD (3, 1, 0.3, 0.1 μM) in cleavage buffer with RNasin RNase Plus Inhibitor (1 Unit/μL; Promega). ^{32}P-labeled PolyU/G RNA oligonucleotide was also incubated with 3 μM *C. elegans* MBP::PGL-1 DD mutants (E442Q, H478A, Q342A). Samples were taken at increasing time points (5, 10, 15, 20, 30, 45, 60, 90, 120 min) and reaction stopped with phenol-chloroform. A no-enzyme sample (dH_20) was incubated 120 min in parallel. A "0" time point represents a sample taken after addition of labeled RNA or DNA to the reaction. Samples were phenol-chloroform extracted and run in sample buffer on 15% (vol/vol) TBE-Urea 0.75-mm mini gels. Gels were fixed, dried, and imaged similar to the *pos-1* and RNA oligo digestion assays. Band intensities were measured using ImageQuant and data presented as ("cleavage product")/("full length oligo" + "cleavage product"). Graphs were generated by Excel and represent an average of three separate experiments.

Double-stranded RNA cleavage assay. ^{32}P-labeled PolyU/G RNA oligonucleotide (1 nM, based on oligo concentration before ^{32}P-labeling) was incubated with unlabeled PolyA/C and PolyU RNA oligonucleotides (Table S2) at 1:10, 1:1, 1:0.1, and 1:0 molar ratios based upon the concentration of PolyU/G used in the initial labeling reaction. Reactions were performed, and samples processed and analyzed similar to time-course assays.

C. elegans. Nematodes were maintained under standard conditions (37). Wild-type was N2 Bristol strain. Mutant alleles were as follows: *IV*: *pgl-1(bn102)* (9); *pgl-1(q842)* (present work) and *pgl-1(q843)* (present work). Strains are as follows: JK5378: *pgl-1(bn102) IV/ nT1[qIs51](IV;V)*, JK5481: *pgl-1(q842) IV/ nT1[qIs51](IV;V)*, and JK5482: *pgl-1(q843) IV/ nT1[qIs51](IV;V)*. The CRISPR/Cas9 coconversion genome-editing approach (38) was used to generate a Q342A mutation in endogenous *pgl-1* (*SI Materials and Methods*); mutants were identified by restriction enzyme digest screening and Sanger sequencing. All CRISPR/Cas9 induced mutants were outcrossed twice with wild-type before analysis. Fertility assays were performed as previously described (8).

ACKNOWLEDGMENTS. The authors thank M. Preston and C. Valley for training; M. Cox for equipment; A. Helsley-Marchbanks for help preparing the manuscript; L. Vanderploeg for help with the figures; and members of the J.K. laboratory, K. Desai, E. Montemayor, T. Nguyen, R. Raines, A. Hoskins, S. Butcher, D. Updike, and S. Strome for helpful discussions. Use of the Life Sciences-Collaborative Access Team Sector 21 was supported by the Michigan Economic Development Corporation and the Michigan Technology Tri-Corridor (Grant 085P1000817). The National Institute of General Medical Sciences and National Cancer Institute Structural Biology Facility at the Advanced Photon Source has been funded in whole or in part with Federal funds from the National Cancer Institute (ACB-12002) and the National Institute of General Medical Sciences (AGM-12006). This research used resources of the Advanced Photon Source, a US DOE Office of Science User Facility operated for the DOE Office of Science by the Argonne National Laboratory under Contract DE-AC02-06CH11357. The Berkeley Center for Structural Biology is supported in part by the National Institutes of Health (NIH), National Institute of General Medical Sciences, and the Howard Hughes Medical Institute. The Advanced Light Source is supported by the Director, Office of Science, Office of Basic Energy Sciences, of the US DOE under Contract DE-AC02-05CH11231. S.T.A. was supported by the Eunice Kennedy Shriver National Institute of Child Health & Human Development of the NIH under Awards F32HD071692 and K99HD081208; C.A.B. was supported by NIH Grants GM094584, GM094622, and GM098248; and M.W. was supported by NIH Grant GM50942. J.K. is an Investigator of the Howard Hughes Medical Institute.

1. Buchan JR, Parker R (2009) Eukaryotic stress granules: The ins and outs of translation. *Mol Cell* 36(6):932–941.
2. Anderson P, Kedersha N (2009) RNA granules: Post-transcriptional and epigenetic modulators of gene expression. *Nat Rev Mol Cell Biol* 10(6):430–436.
3. Brangwynne CP, et al. (2009) Germline P granules are liquid droplets that localize by controlled dissolution/condensation. *Science* 324(5935):1729–1732.
4. Kato M, et al. (2012) Cell-free formation of RNA granules: Low complexity sequence domains form dynamic fibers within hydrogels. *Cell* 149(4):753–767.
5. Voronina E, Seydoux G, Sassone-Corsi P, Nagamori I (2011) RNA granules in germ cells. *Cold Spring Harb Perspect Biol* 3(12):a002774.
6. Ephrussi A, Lehmann R (1992) Induction of germ cell formation by *oskar*. *Nature* 358(6385):387–392.
7. Bontems F, et al. (2009) Bucky ball organizes germ plasm assembly in zebrafish. *Curr Biol* 19(5):414–422.
8. Kawasaki I, et al. (2004) The PGL family proteins associate with germ granules and function redundantly in *Caenorhabditis elegans* germline development. *Genetics* 167(2):645–661.
9. Kawasaki I, et al. (1998) PGL-1, a predicted RNA-binding component of germ granules, is essential for fertility in *C. elegans*. *Cell* 94(5):635–645.
10. Breitwieser W, Markussen FH, Horstmann H, Ephrussi A (1996) Oskar protein interaction with Vasa represents an essential step in polar granule assembly. *Genes Dev* 10(17):2179–2188.
11. Forbes MM, Rothhämel S, Jenny A, Marlow FL (2015) Maternal *dazap2* regulates germ granules by counteracting Dynein in zebrafish primordial germ cells. *Cell Reports* 12(1):49–57.
12. Amiri A, et al. (2001) An isoform of eIF4E is a component of germ granules and is required for spermatogenesis in *C. elegans*. *Development* 128(20):3899–3912.
13. Strome S, Wood WB (1982) Immunofluorescence visualization of germ-line-specific cytoplasmic granules in embryos, larvae, and adults of *Caenorhabditis elegans*. *Proc Natl Acad Sci USA* 79(5):1558–1562.
14. Updike DL, Knutson AK, Egelhofer TA, Campbell AC, Strome S (2014) Germ-granule components prevent somatic development in the *C. elegans* germline. *Curr Biol* 24(9):970–975.
15. Sheth U, Pitt J, Dennis S, Priess JR (2010) Perinuclear P granules are the principal sites of mRNA export in adult *C. elegans* germ cells. *Development* 137(8):1305–1314.
16. Schisa JA, Pitt JN, Priess JR (2001) Analysis of RNA associated with P granules in germ cells of *C. elegans* adults. *Development* 128(8):1287–1298.
17. Hanazawa M, Yonetani M, Sugimoto A (2011) PGL proteins self associate and bind RNPs to mediate germ granule assembly in *C. elegans*. *J Cell Biol* 192(6):929–937.
18. Updike DL, Hachey SJ, Kreher J, Strome S (2011) P granules extend the nuclear pore complex environment in the *C. elegans* germ line. *J Cell Biol* 192(6):939–948.
19. Li S, Yang P, Tian E, Zhang H (2013) Arginine methylation modulates autophagic degradation of PGL granules in *C. elegans*. *Mol Cell* 52(3):421–433.
20. Thandapani P, O'Connor TR, Bailey TL, Richard S (2013) Defining the RGG/RG motif. *Mol Cell* 50(5):613–623.
21. Elbaum-Garfinkle S, et al. (2015) The disordered P granule protein LAF-1 drives phase separation into droplets with tunable viscosity and dynamics. *Proc Natl Acad Sci USA* 112(23):7189–7194.
22. Holm L, Rosenström P (2010) Dali server: Conservation mapping in 3D. *Nucleic Acids Res* 38(Web Server issue):W545–W549.
23. Krissinel E, Henrick K (2007) Inference of macromolecular assemblies from crystalline state. *J Mol Biol* 372(3):774–797.
24. Yoshida H (2001) The ribonuclease T1 family. *Methods Enzymol* 341:28–41.
25. Raines RT (1998) Ribonuclease A. *Chem Rev* 98(3):1045–1066.
26. Yang W (2011) Nucleases: Diversity of structure, function and mechanism. *Q Rev Biophys* 44(1):1–93.
27. Osterman HL, Walz FG, Jr (1978) Subsites and catalytic mechanism of ribonuclease T1: Kinetic studies using GpA, GpC, GpG, and GpU as substrates. *Biochemistry* 17(20):4124–4130.
28. Jeske M, et al. (2015) The crystal structure of the *Drosophila* germline inducer Oskar identifies two domains with distinct Vasa helicase- and RNA-binding activities. *Cell Rep* 12(4):587–598.
29. Matsumoto N, et al. (2015) Crystal structure and activity of the endoribonuclease domain of the piRNA pathway factor Maelstrom. *Cell Reports* 11(3):366–375.
30. Weick EM, Miska EA (2014) piRNAs: From biogenesis to function. *Development* 141(18):3458–3471.
31. Di Tommaso P, et al. (2011) T-Coffee: A web server for the multiple sequence alignment of protein and RNA sequences using structural information and homology extension. *Nucleic Acids Res* 39(Web Server issue):W13–W17.
32. Gibson DG (2011) Enzymatic assembly of overlapping DNA fragments. *Methods Enzymol* 498:349–361.
33. Otwinowski Z, Minor W (1997) Processing of X-ray diffraction data collected in oscillation mode. *Methods Enzymol* 276(Macromolecular Crystallography Part A):307–326.
34. Emsley P, Lohkamp B, Scott WG, Cowtan K (2010) Features and development of *Coot*. *Acta Crystallogr D Biol Crystallogr* 66(Pt 4):486–501.
35. Adams PD, et al. (2010) *PHENIX*: A comprehensive Python-based system for macromolecular structure solution. *Acta Crystallogr D Biol Crystallogr* 66(Pt 2):213–221.
36. McCoy AJ, et al. (2007) *Phaser* crystallographic software. *J Appl Cryst* 40(Pt 4):658–674.
37. Brenner S (1974) The genetics of *Caenorhabditis elegans*. *Genetics* 77(1):71–94.
38. Arribere JA, et al. (2014) Efficient marker-free recovery of custom genetic modifications with CRISPR/Cas9 in *Caenorhabditis elegans*. *Genetics* 198(3):837–846.
39. Dolinsky TJ, Nielsen JE, McCammon JA, Baker NA (2004) PDB2PQR: An automated pipeline for the setup of Poisson-Boltzmann electrostatics calculations. *Nucleic Acids Res* 32(Web Server issue):W665–W667.
40. Grosse-Kunstleve RW, Adams PD (2003) Substructure search procedures for macromolecular structures. *Acta Crystallogr D Biol Crystallogr* 59(Pt 11):1966–1973.
41. McCoy AJ, Storoni LC, Read RJ (2004) Simple algorithm for a maximum-likelihood SAD function. *Acta Crystallogr D Biol Crystallogr* 60(Pt 7):1220–1228.
42. Langer G, Cohen SX, Lamzin VS, Perrakis A (2008) Automated macromolecular model building for X-ray crystallography using ARP/wARP version 7. *Nat Protoc* 3(7):1171–1179.
43. Dickinson DJ, Ward JD, Reiner DJ, Goldstein B (2013) Engineering the *Caenorhabditis elegans* genome using Cas9-triggered homologous recombination. *Nat Methods* 10(10):1028–1034.